Physica Scripta

PAPER

Spark plasma sintering of pure and doped tungsten as plasma facing material

To cite this article: E Autissier *et al* 2014 *Phys. Scr.* **2014** 014034

IOP Publishing | Royal Swedish Academy of Sciences Physica Scripta
Phys. Scr. **T159** (2014) 014034 (4pp) doi:10.1088/0031-8949/2014/T159/014034

Spark plasma sintering of pure and doped tungsten as plasma facing material

E Autissier[1], M Richou[1], L Minier[2], F Naimi[2], G Pintsuk[3] and F Bernard[2]

[1] CEA, IRFM, F-13108 Saint-Paul-Lez-Durance, France
[2] Laboratoire Interdisciplinaire Carnot de Bourgogne, UMR 6303 CNRS-UB, 9 Avenue Alain Savary, BP 47870, F-21078 Dijon Cedex, France
[3] Forschungszentrum Juelich GmbH, EURATOM Association, D-52425 Juelich, Germany

E-mail: emmanuel.autissier@cea.fr

Received 15 May 2013
Accepted for publication 27 September 2013
Published 1 April 2014

Abstract
In the current water cooled divertor concept, tungsten is an armour material and CuCrZr is a structural material. In this work, a fabrication route via a powder metallurgy process such as spark plasma sintering is proposed to fully control the microstructure of W and W composites. The effect of chemical composition (additives) and the powder grain size was investigated. To reduce the sintering temperature, W powders doped with a nano-oxide dispersion of Y_2O_3 are used. Consequently, the sintering temperature for W-oxide dispersed strengthened (1800 °C) is lower than for pure W powder. Edge localized mode tests were performed on pure W and compared to other preparation techniques and showed promising results.

Keywords: spark plasma sintering, tungsten, ODS Y_2O_3, ball milling, edge localized modes

(Some figures may appear in colour only in the online journal)

1. Introduction

Tungsten has been chosen as a plasma facing material in fusion power reactors due to a high melting point, good thermal conductivity, low thermal expansion, high strength at high temperatures and high sputtering threshold energy [1–6]. Moreover, tungsten is a low activating metal. Despite all of its advantages, tungsten exhibits poor ductility and low fracture toughness at low and high temperatures, high-temperature recrystallization brittleness and radiation induced brittleness [7]. The high ductile-to-brittle transition temperature of pure tungsten is the major obstacle during processing and service. Due to its high melting point (3400 °C), its sintering is carried out at high temperature (2500 °C) over several hours to achieve a high density (99.8%). Usually, to obtain the maximum relative density, a supplementary stage is necessary such as hot forging [8]. Nevertheless, the preparation of tungsten at high temperature over a long time leads to a grain growth, which reduces mechanical properties at room temperature by a grain boundary weakening [9]. Grain growth may be limited by stabilizing the microstructure through a dispersion of nanoparticles of refractory materials such as TiC, La_2O_3 and Y_2O_3. The dispersion of oxide-dispersed strengthened (ODS) tungsten materials has also been shown to improve high temperature strength and creep resistance by hindering the grain boundary sliding [10, 11]. Also, finely dispersed particles can act as points of annihilation for radiation induced defects, leading to improved irradiation resistance of the material [12].

Spark plasma sintering (SPS) is one of most attractive techniques for producing innovative materials with a moderate cost and, for some cases, enhanced properties. This fast sintering technique is a high-speed powder consolidation/sintering technology capable of processing conductive and nonconductive materials. SPS consists in simultaneously applying a pulsed direct current of high intensity and a uniaxial pressure to the powder. This very fast process allows the fabrication of materials such as nanostructured materials, functionally graded materials, etc. Moreover, SPS can potentially produce 'near-net shape' and 'net shape' structures directly from powders. In a recent review containing 1005 papers, Orru *et al* [13] report the potentiality of this technology to produce 'in a short time' various types of materials.

The aim of this work is to determine the SPS parameters to obtain a dense pure tungsten sample with regard to the ITER specifications ($d > 98.5\%$). Moreover, in order to reduce the W sintering temperature, the SPS sintering of Y_2O_3–W powder mixtures prepared by ball milling was

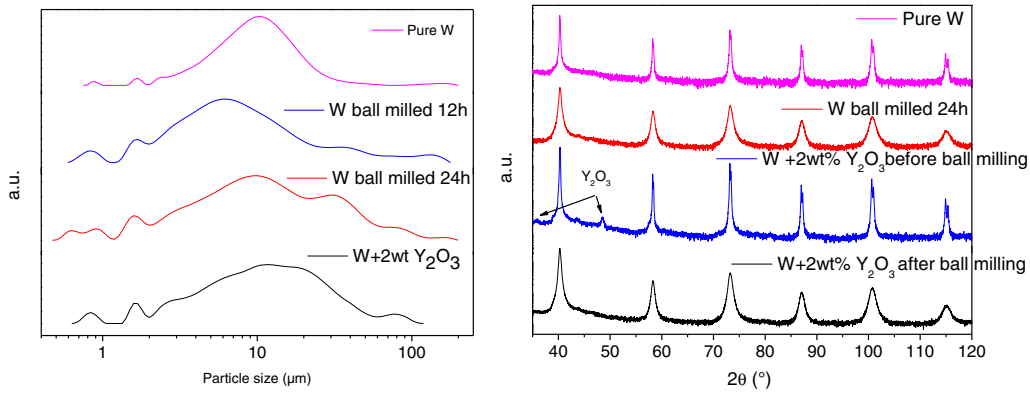

Figure 1. (a) Laser granulometry experiments on pure W, W ball milled 12 h, W ball milled 24 h and W + 2 wtY_2O_3 ball milled 24 h. (b) X-ray diffractometry of pure W, W ball milled during 24 h, W + 2 wt% Y_2O_3 before ball milling and W + 2 wt%Y_2O_3 ball milled during 24 h.

Table 1. Evolution of the grain size in function of relative density for different sintering conditions for pure W.

Temp -erature (°C)	Heating rate (°C min^{-1})	Holding time (min)	Pressure (MPa)	Density (%)	Grain size (μm)
1100	100	10	100	66.3 ± 0.4	2.1 ± 0.2
1300	100	10	100	71.8 ± 0.1	2.3 ± 0.1
1500	100	10	100	81.1 ± 0.3	2.6 ± 0.2
1700	100	10	100	85.6 ± 0.3	2.9 ± 0.2
1900	100	10	100	95.5 ± 0.2	6.6 ± 0.4
1900	50	10	100	89.3 ± 0.7	5.4 ± 0.2
1900	150	10	100	93.2 ± 0.2	7.0 ± 0.4
1900	100	0	100	93.9 ± 0.4	3.4 ± 0.3
1900	100	5	100	93.5 ± 0.3	4.9 ± 0.3
1900	100	20	100	95.2 ± 0.4	6.6 ± 0.4
1900	100	10	50	93.8 ± 0, 4	8.3 ± 0.3

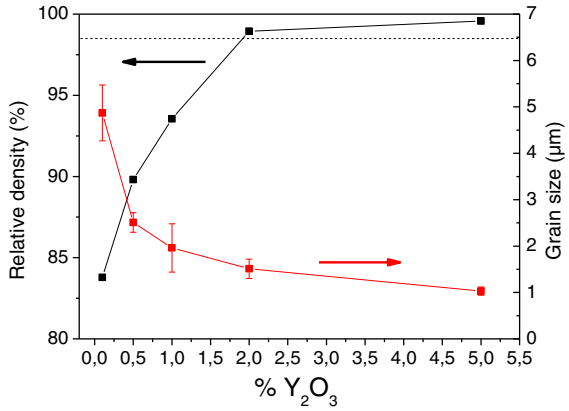

Figure 2. Relative density and grain size in function of wt% Y_2O_3. The dotted line represents the relative density of 98.5%, the ITER specification.

investigated. The Y_2O_3–W SPS sintering has been already studied by El-Atwani *et al* [14], but the diameter of the sample is only 10 mm. In this study the diameter of the sample is three times higher (30 mm), in order to be close to the monoblock geometry. Moreover the density achieved in this study is close to 100%. Finally, thermal shock resistance tests have been performed on this optimized pure tungsten (SPS-W) and compared to a sample prepared by powder injection moulding (PIM).

2. Experimental

2.1. Powder preparation and sintering process

One hundred and thirty grams of commercial W (PTA, 5–10 μm in particle size and 99.5% purity) were ball milled in a planetary ball vario-mill Fritsch Pulverisette 4 [15] composed of two 500 ml vials and 64 balls of 15 mm in diameter both made in tempered iron. In order to protect powders during ball milling, vials are filled with argon. Based on previous works, a specific ball-milling condition was established at 250 rpm (rotations per minute) for the disc rotation speed, −50 rpm for the absolute vial rotation speed. In order to study the influence of the ball-milling time, 12 and 24 h uninterrupted were chosen as ball-milling times. The charge ratio C_R (ball to powder mass ratio) was 7. In fact, in order to limit the powder contamination by the milling tools and to increase simultaneously the yield of mechanical alloying powder mixtures, three millings without cleaning the milling tools were carried out. Under these conditions, the formation of W coating on the vial surface acts as a protective liner against the abrasion on the surface of tempered iron tools and avoids any powder contamination. The same commercial W was mixed during 4 h in a turbula with an Y_2O_3 powder (Alfa Aesar, 30–50 μm in particle size and 99.95% purity). The mixture was then co-milled in the same planetary over 24 h uninterrupted. The oxide content was varied from 0 to 5% (0, 0.1, 0.5, 1, 2 and 5 wt%).

A SPS apparatus HPD 125 (FCT System, Germany) was used to sinter pure SPS-W and doped powders under vacuum (5×10^{-5} bar). Sixty-eight grams of powders were loaded in a graphite mould of 30 mm inner diameter. A graphite foil was inserted between the mould and the powder. In order to establish the sintering map of pure W powder, four parameters such as temperature (1100–1900 °C), pressure (50–100 MPa), holding time (0–20 min) and heating rate (50–150 °C min^{-1}) were investigated. Moreover, the effect of ball milling i.e. the mechanical activation of pure W powder was also studied.

2.2. Characterization

Before characterization, the samples were first polished with 180-grit silicon carbide and up to 1 μm with diamond

Table 2. Summary of ELM results.

	Temperature (°C)	Absorbed power density (GW m^{-2})	State	Deep of cracks (μm)
$n = 100$	20	0.19	No damage	–
	20	0.38	Brittle crack network	≈300
$n = 1000$	20	0.38	Brittle crack network and ductile cracks	≈300
	400	0.38	Roughening and small thermal fatigue cracks	≈25
	700	0.38	Thermal fatigue crack network	≈30

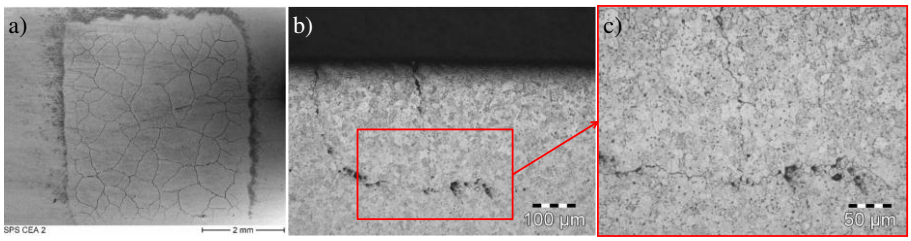

Figure 3. (a) Optical picture of SPS-W, (b) metallographic picture of the SPS (W) and (c) magnification of the red area.

paste and finally cleaned in an ultrasonic ethanol bath in order to remove surface contamination from the graphite foil. The relative density is obtained by the ratio of the bulk density of the sintered samples (determined using the Archimedes method in distilled water) to the theoretical density, obtained using (1). Each value is an average of six measurements. X-ray powder diffraction (XRD) measurements were performed with a Bruker-AXS D8 Advance diffractometer (CuKα radiation, $\lambda = 0.154\,051$ nm) using a super speed VANTEC-1 detector. A scanning electron microscope (SEM JEOL JSM-7600-F) with a field emission gun was used to determine the grain size of samples

$$\rho_{\text{mixture}} = \frac{100}{\frac{\%m_1}{\rho_1} + \frac{\%m_2}{\rho_2}}, \quad (1)$$

with ρ_{mixture} the volumic mass of the mixture, $\%m_1$ the mass percentage of W, ρ_1 the volumic mass of W, $\%m_2$ the mass percentage of Y_2O_3 and ρ_2 the volumic mass of Y_2O_3.

2.3. Edge localized mode (ELM) testing

A thermal shock experiment was performed on SPS-W which has the optimized density in the electron beam facility JUDITH-I [16]. The electron beam provides a diameter at full width half maximum of 1 mm. The loaded area was 4 × 4 mm^2. The sample was exposed to multiple shots (100/1000) at absorbed power densities of 0.19–0.38 GW m^{-2} for 1 ms. The experiment was performed at room temperature (RT), 400 and 700 °C. During testing, surface temperature was monitored using an infrared camera.

3. Result and discussion

3.1. Powder characterizations

Figure 1(a) shows the particle size of all prepared powders including pure W, milled W and W/Y_2O_3 mixtures. The mean grain size of milled powders during 24 h is $1.06 \pm 0.08\,\mu$m (figure 1(a)). The size of the agglomerates increases with the ball milling time. Figure 1(b) shows x-ray patterns of pure W powder and W + 2 wt% Y_2O_3 powder mixture. All XRD peaks correspond to the W phase except for the W + 2 wt% Y_2O_3 before ball milling in which the principal peaks of Y_2O_3 appear. No XRD peak relative to the Y_2O_3 phase is observed after ball milling, certainly due to the good dispersion of Y_2O_3.

3.2. Sintering of pure and doped W

Table 1 shows the evolution of the grain size and the relative density for various sintering parameters. From this table (table 1), it appears that when the sintering temperature was increased both the grain size and the relative density increased. In addition, the evolution of the holding time, the pressure and the heating rate were also investigated in order to reach the maximal densification rate. For example, the role of the heating rate on the grain growth is major, indeed, for 50 °C min^{-1} the grain size is 5.4 μm with a density close to 89.3%, but for a faster heating rate of 150 °C min^{-1} the grain size is larger (7 μm) whereas the densification is stopped at 93.2% still inferior to 95.5% (100 °C min^{-1}). Consequently, the maximum density of pure W obtained is 95.5% for the following conditions: 1900 °C, 100 °C min^{-1}, 10 min and 100 MPa.

When W powders are ball milled, obtained densities are decreased. The densities of the powders ball milled during 12 or 24 h are respectively 84.5 or 87.8%. So the sintering of ball-milled pure W is not sufficient to achieve density equivalent to ITER specifications. The decrease of density can be explained by the fact that, during the high energy ball milling, the crystallite size decreased whereas the defect concentration increased. Consequently the sintering reactivity is changed including a modification of the sintering temperature (beginning and end). Usually, it is not essential to adapt the SPS cycle especially the pressure application to promote the consolidation stage. Moreover, it is also important to limit the oxygen contamination which can form a closed porosity containing a gaseous phase. In addition, due to the heterogeneous grain growth, a "de-densification" stage is observed. During this period pores are created between larger grains due to the rigidity of the W-skeleton. Consequently, in order to increase the density, it is essential not to apply the

mechanical pressure too close to the temperature where the densification velocity is maximal, thereby adding a further driving force. After 1800 °C, the sintering of the 24 h ball milled W powder is achieved. Then, in order to reduce the sintering temperature of pure W powder and simultaneously to increase its relative density, W-ODS powder mixtures containing different amounts of Y_2O_3 were sintered by SPS at 1800 °C during 10 min with a heating of 100 °C min^{-1} and 50 MPa as uniaxial pressure. Figure 2 shows that the relative density increases with the amount of Y_2O_3. For 2 and 5 wt% Y_2O_3, the relative density is above the ITER specifications (98.5%). The grain size of the tungsten decreases with the insertion of Y_2O_3 (figure 2). Indeed, Y_2O_3 is an inhibitor of grain growth. Based on these results, W + 2 wt% Y_2O_3 and W + 5 wt% Y_2O_3 may be candidates for an armoured plasma facing material, in order to respond to the ITER specifications. The sintered density and grain size of W + 2 wt% Y_2O_3 are 98.9% (18 g cm^{-3}) and 1.2 μm respectively.

In order to use this material as an armour material, it will be necessary to test W + 2 wt% Y_2O_3 under ELMs and to measure its thermal conductivity.

3.3. Behaviour of W-SPS under ELMs

Table 2 shows ELM results obtained on the optimized sintered W (SPS-W). For 100 shots (heat flux between 0.19 GW m^{-2} and 0.38 MW m^{-2}, pulse duration of 1 ms, RT), the damage threshold at RT is comparable to other materials [16]. Figure 3(a) represents an optical overview image of the damage area. The area is characterized by a crack network with crack distances in the ramp of 1 mm in the centre and about 500 μm at the edge. Figures 3(b) and (c) show a metallographic cross section of the loaded area. The brittle cracks penetrate to a depth of 300 μm, where the initially vertical cracks tend to deflect in a direction parallel to the surface. This is triggered by the stress field induced by the steep temperature gradient and the tendency of the cracks to follow weak grain boundaries. When increasing the pulse number at RT from 100 to 1000, in addition to the brittle cracks, thermal fatigue cracks with a crack length inferior to 80 μm are observed. In addition to brittle cracks, roughening and very small cracks are generated. Increasing the base temperature to 700 °C, the damage significantly increases and thermal fatigue network are formed. Furthermore, it is worth mentioning, that in the surface region where thermal fatigue cracking occurs there is a change in microstructure (grain refinement). This is probably a result of the plastic deformation caused by the thermal cycling. Under similar ELM test conditions similar damages were observed for W manufactured with PIM-W.

4. Conclusion

The optimized SPS parameters for pure tungsten are 1900 °C, 10 min and 100 °C min^{-1}, under 100 MPa without ball milling. A thermal shock experiment was performed on a SPS-W. Even if the relative density of the pure SPS-W sample is still low (95.5%) compared to PIM-W, their behaviours are very similar. Due to its porosity, SPS-W shows a relatively week thermal fatigue resistance. W-based alloys containing a dispersion of Y_2O_3 nano oxide powders have been prepared by high energy ball milling during 24 h. Then, the W-ODS powder mixture is sintered by SPS according to the following condition: sintering at 1800 C during 10 min, at 100 °C min^{-1} and 50 MPa. The dispersing oxide Y_2O_3 acts as an inhibitor of grain growth and increases the relative density. The W-2 wt% Y_2O_3 prepared by SPS seems an interesting candidate when considering its density (98.9%).

References

[1] Garcia-Rosales C 1994 *J. Nucl. Mater.* **211** 202–14
[2] Norajitra P *et al* 2004 *J. Nucl Mater.* **329–333** 1594–8
[3] Tanabe T, Noda N and Nakamura H 1992 *J. Nucl Mater.* **196** 11–27
[4] Diegele E, Krüssmann R, Malang S, Norajitra P and Rizzi G 2003 *Fusion Eng. Des.* **66–68** 383–7
[5] Chuynaov V 1996 *J. Nucl. Mater.* **233–237** 4–8
[6] Cottrell G 2006 *Mater Sci. Technol.* **22** 869–80
[7] Smid I, Akiba M, Vieider G and Plöchl L 1998 *J. Nucl. Mater.* **258–263** 160–72
[8] Kitsunai Y, Kurishita H, Kayano H, Hiraoka Y, Igarashi T and Takida T 1999 *J. Nucl. Mater.* **271–272** 423–8
[9] Babak A 1983 *Powder Metall. Met. Ceram.* **22** 316–8
[10] Rose M, Balogh A and Hahn H 1997 *Nucl. Instrum. Methods Phys. Res.* B **127–128** 119–22
[11] Radiguet B, Etienne A, Pareige P, Sauvage X and Valiev R 2008 *J. Mater. Sci.* **43** 7338–43
[12] Wurster S and Pippan R 2009 *Scr. Mater.* **60** 1083–7
[13] Orrù R, Licheri R, Locci A, Cincoti A and Cao G 2009 *Mater. Sci. Eng.* R **63** 127–287
[14] El-Atwani O, Quach D, Efe M, Cantwell P, Heim B, Schultz B, Stach E, Groza J and Allain J 2011 *Mater. Sci. Eng.* A **528** 5670–7
[15] Abdellaoui M and Gaffet E 1995 *Acta Metall. Mater.* **43** 1087–98
[16] Loewenhoff T, Hirai T, Keusemann S, Linke J, Pintsuk G and Schmidt A 2011 *J. Nucl. Mater.* **415** S51–4